

Unsupervised Domain Adaptation for Video Semantic Segmentation

Kwanyong Park* Inkyu Shin* Sanghyun Woo In So Kweon
KAIST, South Korea.

{pkyong7,dlsrbgg33,shwoo93,iskweon77}@kaist.ac.kr

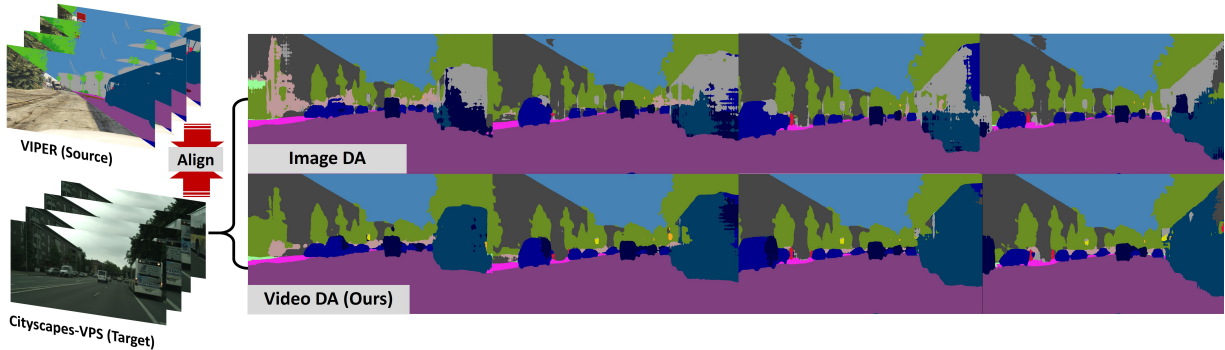


Figure 1: **Adaptation outputs on VIPER to Cityscapes-VPS.** We compare our method with the state-of-the-art Image DA method (Mei et al. 2020). It is readily apparent that our predictions are more semantically accurate and temporally consistent.

Abstract

Unsupervised Domain Adaptation for semantic segmentation has gained immense popularity since it can transfer knowledge from simulation to real (Sim2Real) by largely cutting out the laborious per pixel labeling efforts at real. In this work, we present a new video extension of this task, namely **Unsupervised Domain Adaptation for Video Semantic Segmentation**. As it became easy to obtain large-scale video labels through simulation, maximizing Sim2Real knowledge transferability is one of the promising directions for resolving the fundamental data-hungry issue in the video. To tackle this new problem, we present a novel video-specific two-phase adaptation scheme. In the first step, we train the model using labeled source videos and align the features from source to target with the guidance of video context. In the second step, we train the model on target videos using pseudo labels. To obtain dense and accurate pseudo labels, we exploit the temporal information in the video. By combining these two steps, we construct a solid video adaptation method. On the ‘VIPER to CityscapeVPS’ adaptation scenario, we show that our proposals significantly outperform all the previous image-based UDA methods both on image-level (mIoU) and video-level (VPQ^s) evaluation metrics.

Introduction

A pixel-level understanding of different semantics, object instances, and temporal changes in a video provides primitive information for various vision applications such as autonomous driving, robot control, and augmented reality. Video semantic segmentation has been regarded as one of the representative proxies for this challenging goal. While

a large number of learning-based approaches under two main research directions of improving accuracy (Nilsson and Sminchisescu 2017; Li, Shi, and Lin 2018) and efficiency (Shelhamer et al. 2016; Zhu et al. 2017) have been presented, the scarcity of the available video labels turns out to be the bottleneck of further advances in this field.

Recently, simulators based on video game engines, which can quickly generate an unlimited amount of high-quality, diverse video labels, emerged as an attractive alternative for laborious human labeling. However, the model trained on simulated data suffers from the fundamental *domain shift* (Sankaranarayanan et al. 2018), and thus the severe performance drop in the real world is inevitable without proper adaptation. To remedy these distribution shifts, the community has put a great effort into developing domain adaptation techniques. While there has been a flurry of advances, most of the previous studies overlook temporal context that limits adaptation still to an *image level* and thus cannot scale to video model adaptation.

In this work, we present a novel video-specific adaptation method that is comprised of two phases. The first phase is an adversarial video training (VAT) step that uses video context to train the model and align the features from source to target. Specifically, a tube matching loss is introduced to explicitly capture temporal changes of shape and boundaries of each segment. Also, a sequence discriminator is presented to adapt the features better using spatio-temporal information. The second phase is a video self-training (VST) step that focuses on the target data learning with the generated pseudo labels. To obtain more dense and accurate pseudo labels, we aggregate information from the neighboring frames. We show that these two phases are complementary and form a compelling video adaptation method, which sets strong

*equal contribution

baseline scores on challenging VIPER (Richter, Hayder, and Koltun 2017) to CityscapeVPS (Kim et al. 2020) adaptation scenario. We summarize our contributions as follows:

1. We firstly define and explore unsupervised domain adaptation for video semantic segmentation.
2. We design a novel two-phase video domain adaptation scheme. The two main components are Video Adversarial Training (VAT) and Video Self Training (VST). We show that both are essential and complementary in constructing a compelling video adaptation method.
3. We validate our proposal on the Viper to CityscapeVPS scenario. We show that our method significantly outperforms all the previous image-based UDA approaches both on image-specific (mIoU) and video-specific (VPQ (Kim et al. 2020)) evaluation metrics. Our results clearly show the importance of developing video-specific adaptation techniques.

Related Works

Domain Adaptive Semantic Segmentation

A number of domain adaptation techniques have been studied in various vision tasks. Among them, domain adaptive semantic segmentation, which requires the challenging adaptation of structured output at a pixel level. There are two dominant paradigms in this field: *Adversarial learning-based* (Tsai et al. 2018; Yu et al. 2019; Wang et al. 2020) and *Self-training-based* (Zou et al. 2018, 2019). Some works investigated combining these two methods to reduce the domain gap further (Li, Yuan, and Vasconcelos 2019; Pan et al. 2020; Shin et al. 2020; Mei et al. 2020). However, we note these methods are still limited at *image-level* adaptation, which cannot scale to video-level adaptation as it overlooks important temporal information. Recently, (Chen et al. 2020) attempted to utilize information across the frames for binary segmentation of medical images. However, its framework neither aims for video segmentation nor employs explicit temporal feature aggregations, which we empirically show that it is inferior to our framework on complex urban scene video segmentation¹. In this work, we carefully designed a two-phase video adaptation framework that *explicitly* aggregates and utilizes temporal information, which has been rarely studied in earlier works.

Video Semantic Segmentation

A dense understanding of video is one of the long-standing fundamental vision problems that have various applications. As a representative proxy, video semantic segmentation has been actively studied to improve accuracy and efficiency. However, most current video segmentation benchmarks provide annotations for only a single frame per video clip (Cordts et al. 2016; Yu et al. 2020), mainly due to laborious dense labeling efforts. We instead explore video simulated learning, which allows us to avoid expensive manual labeling, and propose a strong video adaptation method.

¹We provide detailed analysis in the supplementary material.

Preliminary

For better understanding of our proposals, we provide preliminaries based on the state-of-the-art image domain adaptive segmentation framework, IAST (Mei et al. 2020).

Problem Setting in image UDA

We assume that both the data and labels, $(x_s, y_s) \in (\mathbf{X}_S, \mathbf{Y}_S)$, are available in source domain. In contrast, the data, $x_t \in \mathbf{X}_T$, is only available in target domain.

Image Adversarial training(IAT)

Adversarial training in image DA can be conducted via minimizing source-specific segmentation loss and generative adversarial loss. We denote G , $P_s = G(x_s)$ and $P_t = G(x_t)$ as semantic segmentation network, predicted source, and target segmentation map, respectively. Source-specific segmentation loss is defined as $L_{seg}(P_s, y_s)$, where L_{seg} is cross-entropy.

To align the distribution between source and target image, adversarial learning (Tsai et al. 2018) is applied.

$$\mathcal{L}_{Adv,I}(G, D_I) = \mathbb{E}_{\mathbf{x}_s \sim X_S} [\log D_I(P_s)] + \mathbb{E}_{\mathbf{x}_t \sim X_T} [\log(1 - D_I(P_t))] \quad (1)$$

A image discriminator D_I tries to discriminate between target segmentation map P_t and source segmentation map P_s , while the segmentation network G attempts to fool the discriminator. Therefore, full objective function in IAT can be summarized as below:

$$L_{IAT}(G, D_I) = L_{seg}(P_s, y_s) + \lambda_{Adv} \mathcal{L}_{Adv,I}(G, D_I) \quad (2)$$

Image Self training(IST)

Self-training iteratively generates pseudo labels and re-trains the model. In typical, the pseudo label \hat{y}_t can be formulated as

$$\hat{y}_t^{(k)} = \arg \max_{k \in K} \mathbb{1}_{P_t^{(k)} > \theta^{(k)}} P_t^{(k)} \quad (3)$$

where $\mathbb{1}$ is a function which returns the input if the condition is true or ignored otherwise. $\hat{y}_t^{(k)}$ and $P_t^{(k)}$ are pseudo label and prediction for class k , respectively. When the confidence is above a certain threshold $\theta^{(k)}$, the predicted class is selected as a pseudo label.

Defining proper threshold $\theta^{(k)}$ is crucial for cutting out the noisy pseudo labels. In practice, IAST (Mei et al. 2020) adjusts it for each images to diversify the pseudo labels. The threshold of current image $\theta_t^{(k)}$, is decided as follows:

$$\theta_t^{(k)} = \beta \theta_{t-1}^{(k)} + (1 - \beta) \Psi(x_t, \theta_{t-1}^{(k)}), \quad (4)$$

$$\Psi(x_t, \theta_{t-1}^{(k)}) = \mathbb{P}_t^{(k)} [\alpha \theta_{t-1}^{(k) \gamma} | \mathbb{P}_t^{(k)} |]$$

$\theta_t^{(k)}$ is a moving averaged threshold with a momentum factor β . $\Psi(x_t, \theta_{t-1}^{(k)})$ represents the threshold for acquiring the current instance. α controls the proportion of pseudo labels, and γ is a weight decay parameter to reduce pseudo labels with low confidence.

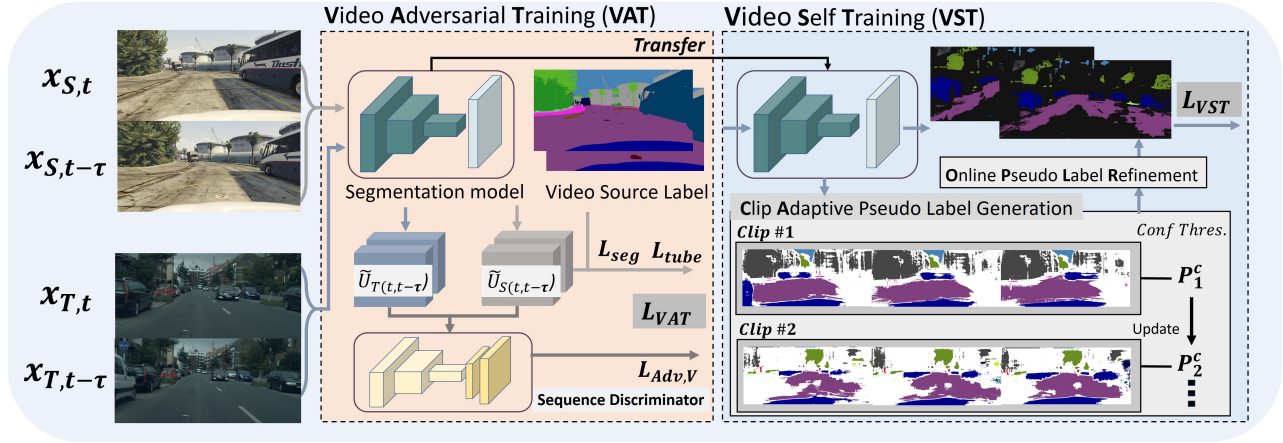


Figure 2: **The overview of the proposed unsupervised domain adaptation for video semantic segmentation (Video DA).** Our Video DA consists of two phase video specific domain adaptation training: Video Adversarial Training (VAT) and Video Self Training (VST). In first phase, VAT, we stack two neighbor outputs from two domains ($U_{S(t,t-\tau)}$ for source and $U_{T(t,t-\tau)}$ for target) and utilize sequence discriminator to align them. In second phase, VST, we design a aggregation based clip adaptive pseudo label generation strategy.

Given pseudo labels on the target domain, the image self-training loss can be defined as:

$$L_{IST}(G) = \lambda_{seg,s} L_{seg}(P_s, y_s) + \lambda_{seg,t} L_{seg}(P_t, \hat{y}_t) + \lambda_{reg} L_{reg}(P_t, \hat{y}_t) \quad (5)$$

The third term represents additional regularization for self-training (Zou et al. 2019; Mei et al. 2020). For more details, please refer to the original papers.

Methods

Problem Setting in Video UDA

Video domain adaptation aims to transfer space-time knowledge from labeled source domain S to the unlabeled target domain T . Different from the single frame setting in image UDA, source set consists of temporally ordered frame sequences, $x_S := \{x_{S,1}, x_{S,2}, \dots, x_{S,t}, \dots\}$ ($x_S \in \mathbf{X}_S$), and corresponding label sequences, $y_S := \{y_{S,1}, y_{S,2}, \dots, y_{S,t}, \dots\}$ ($y_S \in \mathbf{Y}_S$). In the target domain, we have data without labels. We denote target frame sequences as $x_T := \{x_{T,1}, x_{T,2}, \dots, x_{T,t}, \dots\}$ ($x_T \in \mathbf{X}_T$).

Overview of Proposed Method

Unlike static images, videos have rich temporal and motion information. To train a model with such information, we propose a novel two-phase approach that is consisted of video adversarial training (VAT) and video self-training (VST). In the VAT step, the model learns source domain knowledge using video labels, and adapts its features from source to target. In the VST step, the model directly learns target domain knowledge based on the generated pseudo labels. We note that *video context* is explicitly utilized in both steps. Fig. 2 shows the overview of the proposed method. We detail each step in the following sections.

Video Adversarial Training (VAT)

In this step, we aim to learn source domain knowledge using video labels and adapt the features from source to target via adversarial loss. Specifically, given input source frames $x_{S,t}$, $x_{S,t-\tau}$ from time t and $t-\tau$, the image semantic segmentation model G predicts “soft-segmentation map” $P_{S,t}$, $P_{S,t-\tau}$. A conventional frame-level semantic segmentation is learned from applying the standard cross-entropy loss to each frames.

We further leverage source labels and designed a new video level supervision signal, tube matching loss, that can capture the finer temporal changes of each segment. Also, to facilitate the adversarial learning with the additional temporal context, we present sequence discriminator. We detail each in the following.

Tube Matching Loss Training a model with each frame independently apparently misses rich temporal information. Here, we propose a novel tube matching loss that compares the tube prediction of each class with the groundtruth tube, which aims to capture and correct the boundary and shape changes of every segment in the video. We consider two-length tube in this paper due to the GPU memory limit. In particular, we denote $\tilde{U}_{S(t,t-\tau)} = [P_{S,t}, P_{S,t-\tau}]$ as the sequence of source prediction that is a concatenation of two soft segmentation maps in temporal dimension. $\tilde{U}_{S(t,t-\tau)}^{(k)} = [P_{S,t}^{(k)}, P_{S,t-\tau}^{(k)}]$ is a segment tube of class k . Groundtruth tube $U_{S(t,t-\tau)}^{(k)}$ is defined similarly. The tube matching loss is instantiated with the dice coefficient (Milletari, Navab, and Ahmadi 2016) between the prediction $\tilde{U}_{S(t,t-\tau)}$ and groundtruth $U_{S(t,t-\tau)}$.

$$\mathcal{L}_{tube}(\tilde{U}_{S(t,t-\tau)}, U_{S(t,t-\tau)}) = \sum_{k=1}^K [1 - Dice(\tilde{U}_{S(t,t-\tau)}^{(k)}, U_{S(t,t-\tau)}^{(k)})] \quad (6)$$

The dice coefficient is insensitive to number of each class prediction and defined as

$$Dice(p, q) = \frac{2 \sum (pq)}{\sum p^2 + \sum q^2} \quad (7)$$

We empirically show that the tube matching loss allows the model to learn more discriminative feature compared to the baseline model trained only with the standard frame-level cross-entropy loss, indicating that incorporating the temporal context in feature learning is crucial.

Sequence Discriminator To alleviate domain discrepancy both in space and time, we propose to use sequence discriminator. Different from image discriminator (Tsai et al. 2018; Vu et al. 2019), sequence discriminator D_V takes sequence of soft segmentation maps as an input. The discriminator is trained to discriminate sequence of source and target. At the same time, the segmentation model attempts to fool the discriminator. The video GAN loss is as follows:

$$L_{Adv,V}(G, D_V) = \mathbb{E}_{\mathbf{x}_{S,t}, \mathbf{x}_{S,t-\tau} \sim X_S} \left[\log D_V(\tilde{U}_{S(t,t-\tau)}) \right] + \mathbb{E}_{\mathbf{x}_{T,t}, \mathbf{x}_{T,t-\tau} \sim X_T} \left[\log(1 - D_V(\tilde{U}_{T(t,t-\tau)})) \right] \quad (8)$$

where $\tilde{U}_{T(t,t-\tau)}$ is sequence of prediction on target images, $x_{T,t}$ and $x_{T,t-\tau}$. By construction, the semantic segmentation model learns to align sequence distribution between source and target.

Full objective function for VAT Total loss function is defined as

$$L_{VAT}(G, D_v) = \sum_{l=t,t-\tau} [\mathcal{L}_{seg}(P_{S,l}, y_{S,l})] \quad (9) + \mathcal{L}_{tube}(\tilde{U}_{S(t,t-\tau)}, U_{S(t,t-\tau)}) + \lambda_V \mathcal{L}_{Adv,V}(G, D_V)$$

Along with per-frame cross entropy loss, the tube matching loss enforce model to produce accurate and consistent prediction on source domain, while video gan loss adapts the learned representation to the target domain.

Video Self Training(VST)

Different from previous methods (Zou et al. 2018; Mei et al. 2020) that treat each image independently, we predict pseudo label at the clip level as a whole which leads to robustly cut-out the noisy predictions. In the training time, we additionally conduct the pseudo label refinement step to further eliminate error in the pseudo label. To benefit from temporal information both in *pseudo label generation* and *pseudo label refinement*, we aggregate predictions and employ temporal consensus of pseudo label across the different time steps.

Temporally Aggregated Prediction In pseudo label generation step, we take two neighbor frames $x_{T,j}$ ($j \in \{i-1, i+1\}$), to aggregate their predictions onto a target frames, $x_{T,i}$. Given a target frame $x_{T,i}$ and a neighbor frame $x_{T,j}$, pixel-level correspondence is estimated by an optical flow network(e.g. FlowNet2.0 (Ilg et al. 2016)). The predicted

Algorithm 1: Pseudo Label Generation

Input: Model G , $[x_T = \{x_{T,1}, x_{T,2}, \dots, x_{T,t}, \dots\}]_{T=1}^N$
Parameter: proportion α , momentum β
Output: target video pseudo-labels

```

1: init  $\theta_0=0.9$ 
2: for  $T=1$  to  $N$  do
3:    $\tilde{U}_{T(1:N)}^A = \text{Aggregate}(G(x_T))$  /// $\text{Eq. (10)}$   $\text{*/}$ 
4:    $\tilde{U}_{index} = \arg \max(\tilde{U}_{T(1:N)}^A)$ 
5:    $\tilde{U}_{value} = \max(\tilde{U}_{T(1:N)}^A)$ 
6:   for  $k$  in  $K$  do
7:      $\tilde{U}_T^{(k)} = \text{sort}(\tilde{U}_{value}[\tilde{U}_{index} = k])$ 
8:      $\theta_{x_T}^{(k)} = \Psi(x_T, \theta_{T-1}^{(k)})$  /// $\text{Eq. (11)}$   $\text{*/}$ 
9:   end for
10:   $\theta_T = \beta \theta_{T-1} + (1 - \beta) \theta_{x_T}$  /// $\text{Eq. (11)}$   $\text{*/}$ 
11:   $\hat{y}_T = \text{onehot}(\tilde{U}_{index}[\tilde{U}_{value} > \theta_T])$ 
12: end for
13: return  $[\hat{y}_T]_{T=1}^N$ 

```

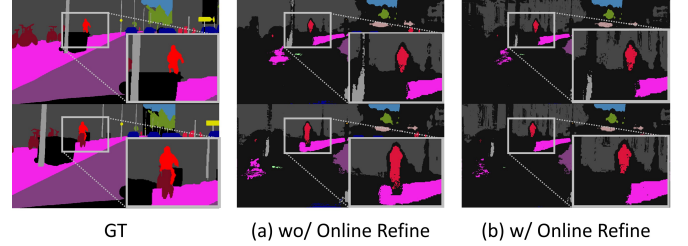


Figure 3: **Visualization of pseudo-labels w/o and w/ the online refinement.** The proposed online refinement successfully eliminate noise on the pseudo labels by checking temporal consensus.

soft-segmentation maps on the neighbor frame are warped to the target frame as follows. To aggregate diverse prediction from multiple frames, we average the predictions from target and neighbor frame when the warped prediction is not occluded. The non-occluded map from $x_{T,j}$ to $x_{T,i}$ is defined by $\mathbb{I}_{j \Rightarrow i} = \{1 | O_{j \Rightarrow i} > th\}$ where th is threshold value and $O_{t \Rightarrow t-1} = \exp(-\alpha \|x_{T,i} - W_{j \Rightarrow i}(x_{T,j})\|_2)$ denotes the occlusion mask which is calculated from the warping error between target frame $x_{T,i}$ and warped neighbor frame $W_{j \Rightarrow i}(x_{T,j})$. The aggregated prediction at target frame is computed as,

$$P_{T,i}^A = \frac{P_{T,i} + \sum_j \mathbb{I}_{j \Rightarrow i} W_{j \Rightarrow i}(P_{T,j})}{1 + \sum_j \mathbb{I}_{j \Rightarrow i}} \quad (10)$$

Thus, sequence of aggregated prediction for a clip x_T is expressed as, $\tilde{U}_{T(1:N)}^A = [P_{T,1}^A, P_{T,2}^A, \dots, P_{T,t}^A, \dots]$ where N represent total frame number of each clip. We abbreviate above process as *Aggregate*.

Clip Adaptive Pseudo Label Generation As consecutive frames share a large amount of redundant information, we

VIPER → Cityscapes-VPS [mIoU]																	
Method	Arch.	RD	SW	BD	FN	PL	TL	TS	Veg.	TR	SKY	PR	Car	Truck	Bus	Motor	mIoU(%)
Source-only	-	44.24	22.70	73.69	6.02	6.74	10.47	19.25	82.55	31.13	80.74	60.91	62.37	2.25	7.18	0.0	34.02
AdaptSegNet (Tsai et al. 2018)	AT	86.09	41.54	80.59	16.10	12.71	20.00	23.98	82.44	34.05	80.14	64.79	69.23	6.41	4.15	0.0	41.48
Advent (Vu et al. 2019)	AT	87.10	42.27	80.57	18.46	12.90	21.69	24.88	82.22	31.87	79.82	65.88	74.53	6.83	7.32	0.0	42.42
CBST (Zou et al. 2018)	ST	27.09	27.00	80.83	13.88	2.55	24.01	18.10	82.95	48.69	82.84	61.29	73.29	23.71	5.91	0.0	38.14
CRST (Zou et al. 2019)	ST	25.52	23.71	81.15	18.85	3.02	25.57	20.39	83.01	46.66	80.91	63.06	74.65	22.76	12.38	0.52	38.81
CCM (Li et al. 2020)	ST	87.02	46.76	80.78	32.50	11.25	33.60	26.84	84.09	42.65	82.14	68.36	72.89	10.35	3.69	0.0	45.52
FDA (Yang and Soatto 2020)	ST	81.63	40.89	82.38	50.95	11.23	22.94	28.23	82.50	49.43	81.16	59.79	70.73	11.12	18.97	0.0	46.13
IntraDA (Pan et al. 2020)	A+S	89.82	49.00	83.20	26.46	15.69	21.32	23.80	83.34	42.13	74.49	68.45	75.62	8.53	11.31	0.0	44.88
CBST* (Zou et al. 2018)	A+S	88.70	56.66	82.88	32.16	17.59	32.30	19.38	83.80	40.74	74.57	69.68	69.00	17.77	12.32	00.83	46.56
CRST* (Zou et al. 2019)	A+S	88.73	56.64	83.04	31.66	17.79	33.89	19.02	83.98	40.00	75.00	70.82	69.60	18.48	12.34	1.38	46.83
IAST (Mei et al. 2020)	A+S	91.35	62.29	85.55	35.75	19.62	36.51	27.26	86.10	38.98	84.36	70.89	73.03	13.33	14.43	0.90	49.36
Ours	A+S	91.23	53.99	85.86	35.90	18.73	43.43	34.97	86.28	36.09	86.01	65.61	81.81	21.74	34.91	2.04	51.91
Oracle	-	94.98	67.68	87.42	61.10	32.20	40.71	56.11	86.82	55.76	87.47	70.22	89.55	51.65	73.43	0.71	63.72

Table 1: Image semantic segmentation results(mIoU).

VIPER → Cityscapes-VPS [VPQ ^s]																	
Method	Arch.	RD	SW	BD	FN	PL	TL	TS	Veg.	TR	SKY	PR	Car	Truck	Bus	Motor	mIoU(%)
Source-only	-	28.55	3.84	65.95	0.45	0.0	0.1	5.37	75.22	5.50	64.29	18.38	48.50	1.34	0.0	0.0	21.17
AdaptSegNet (Tsai et al. 2018)	AT	84.97	18.90	75.87	4.66	0.05	2.98	8.02	74.76	6.69	65.26	20.85	59.02	2.19	0.0	0.0	28.28
Advent (Vu et al. 2019)	AT	85.55	20.02	74.59	6.90	0.27	3.31	8.04	74.70	6.66	65.64	22.80	65.84	2.03	0.14	0.0	29.10
CBST (Zou et al. 2018)	ST	5.56	8.60	74.88	7.05	0.05	3.14	5.27	75.53	12.31	67.83	21.71	61.30	4.72	0.0	0.0	23.20
CRST (Zou et al. 2019)	ST	5.63	6.51	76.27	5.89	0.07	3.21	5.74	75.29	11.06	64.11	24.73	62.37	6.42	1.56	0.0	23.26
CCM (Li et al. 2020)	ST	85.59	28.19	75.71	8.34	0.10	3.44	8.88	77.60	8.81	70.81	27.54	62.54	5.06	0.0	0.0	30.84
FDA (Yang and Soatto 2020)	ST	78.78	22.03	77.92	16.90	0.35	0.44	5.70	75.76	11.96	67.15	25.29	58.08	3.77	1.45	0.0	29.70
IntraDA (Pan et al. 2020)	A+S	89.44	29.12	78.26	9.02	0.97	0.79	7.62	78.18	11.19	62.35	28.26	65.56	5.76	0.26	0.0	31.12
CBST* (Zou et al. 2018)	A+S	87.67	41.12	78.66	10.39	0.88	6.47	3.86	77.97	10.28	51.52	29.53	56.88	5.36	0.0	0.0	30.71
CRST* (Zou et al. 2019)	A+S	87.74	41.80	78.81	9.90	1.03	8.16	3.63	78.18	10.87	52.07	30.02	57.50	5.58	0.0	0.35	31.04
IAST (Mei et al. 2020)	A+S	90.06	45.86	82.54	14.63	2.60	6.98	8.00	80.78	14.84	70.21	34.56	62.84	5.51	1.04	0.19	34.71
Ours	A+S	90.64	37.32	82.68	11.31	2.46	10.76	14.40	81.20	13.97	75.42	32.68	74.89	9.30	9.37	0.0	36.43
Oracle	-	94.81	49.98	84.24	23.16	4.37	7.10	28.58	80.40	17.73	73.84	32.84	78.63	10.57	35.00	0.0	41.42

Table 2: Video semantic segmentation results(VPQ^s).

define each clip after *Aggregate* process as a single instance. The threshold of current clip $\theta_t^{(k)}$, for class k, is defined as follows:

$$\begin{aligned} \theta_t^{(k)} &= \beta\theta_{t-1}^{(k)} + (1 - \beta)\Psi(x_T, \theta_{t-1}^{(k)}), \\ \Psi(x_T, \theta_{t-1}^{(k)}) &= \tilde{\mathcal{U}}_T^{(k)}[\alpha\theta_{t-1}^{(k)\gamma} | \tilde{\mathcal{U}}_T^{(k)}] \end{aligned} \quad (11)$$

The same threshold $\theta_t^{(k)}$ is adopted to each frame, which is exponential moving average between threshold of previous clip $\theta_{t-1}^{(k)}$ and $\Psi(x_T, \theta_{t-1}^{(k)})$. $\Psi(x_T, \theta_{t-1}^{(k)})$ is acquired similar to IAST, while the operating unit is sequence of predictions rather than a prediction of single image. The overall pseudo label generation is summarized in Algorithm. 1.

Full objective function for VST Overall loss function is expressed as

$$\begin{aligned} L_{VST}(G) &= \sum_{l=t, t-\tau} [L_{seg}(P_{T,l}, RF(\hat{y}_{T,l})) \\ &+ \lambda_{reg} L_{reg}(P_{T,l}, RF(\hat{y}_{T,l}))] \end{aligned} \quad (12)$$

Pseudo Label Refinement via Temporal Consensus

Corresponding pixels across the video should belongs to the same class. However, in practice, it is not always held on the pseudo labels. To eliminate such noise in pseudo label level, we implement pseudo label refinement with temporal correspondence. Specifically, reference pseudo label $\hat{y}_{T, t-\tau}$ is warped onto current pseudo label $\hat{y}_{T, t}$ and check the consensus between them. If not, the model is not learned from the region. The refined current pseudo label $RF(\hat{y}_{T, t})$ can be formulated as follow:

$$RF(\hat{y}_{T, t}) = \mathbb{1}_{[\hat{y}_{T, t} = W_{t-\tau \Rightarrow t}(\hat{y}_{T, t-\tau})]} \hat{y}_{T, t} \quad (13)$$

Experiments

Experimental settings

Datasets We evaluate our video domain adaptation framework on the synthetic-to-real scenarios: VIPER (Richter, Hayder, and Koltun 2017) to Cityscapes-VPS (Kim et al. 2020). The VIPER dataset has 254,064 video frames and corresponding semantic labels. We only take 42455 images on “day” conditions as training data. Cityscape-VPS is video-level extension of Cityscapes dataset (Cordts et al. 2016), which further annotate 5 frames out of each 30-frames video clip. Following official split in (Kim et al. 2020), we use 400 clips to train a model and evaluated on 50 validation sequences.

Baselines We compare our methods with several baselines. (1) Source-only is a model naively trained on source domain. (2) Adversarial based image UDA methods include AdaptSegNet (Tsai et al. 2018), Advent (Vu et al. 2019) which rely solely on GAN based adversarial training. (3) Self-training based image UDA methods, CBST (Zou et al. 2018), CRST (Zou et al. 2019), CCM (Li et al. 2020) and FDA (Yang and Soatto 2020), iteratively generate pseudo-labels and retrain the models. (4) Advanced methods such as IntraDA (Pan et al. 2020) and IAST (Mei et al. 2020) combine adversarial and self-training. In addition, we build strong baselines, CBST* and CRST*, by applying each methods on top of adversarially adapted model that is used in IAST.

Evaluation Metric The predicted results should be both accurate as groundtruth and consistent in time. We first evaluate image-level semantic segmentation performance using standard mean intersection of union(mIoU). In addition, we

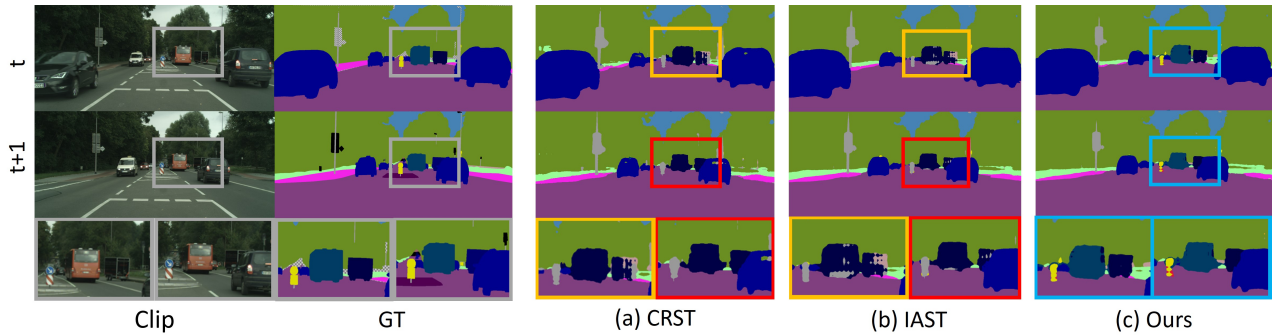


Figure 4: **Qualitative comparison with the baselines.** We indicate yellow and red boxes for inaccurate and inconsistent prediction, respectively. We can see that previous approaches suffer from both wrong and temporally inconsistent prediction. Instead, our framework successfully resolves both issues. Best viewed in color.

borrow the video panoptic quality (VPQ) (Kim et al. 2020) to measure the video-level accuracy. To fit the task of video semantic segmentation, we view the prediction of each class as single instance (i.e. stuff) when the video panoptic quality is calculated. We call the modified VPQ metric VPQ^s in this paper. We measure mIoU and VPQ^s on 15 common classes.

Implementation details Motivated by (Liu et al. 2020), we adopt image semantic segmentation models and process each video frame independently for inference. We use a pre-trained ResNet-50 (He et al. 2015) as backbone network and adapt DeepLabv2 (Chen et al. 2017) as semantic segmentation head. Due to the limitation of GPU memory, we randomly select 2 consecutive frames during training. From the image discriminator architecture in (Tsai et al. 2018; Vu et al. 2019), we replace the first 2D convolution layer with 3D convolution layer of temporal stride 2. This modification allows the discriminator D_V to take sequence of predictions as input. We set th to 0.7 for cutting out the occluded area.

Comparison with State-of-the-art

In Table. 1 and Table. 2, we report the quantitative adaptation performance on VIPER to Cityscapes-VPS. We compare proposed method with Source-only model, state-of-the-art image UDA-models including adversarial based (Tsai et al. 2018; Vu et al. 2019), self-training based (Zou et al. 2018, 2019), and combined methods (Mei et al. 2020).

For image-level evaluation, proposed method shows best mIoU 51.91% with healthy margin. For example, we boost the state-of-the-art image-level UDA method, IAST, by +2.55% mIoU. It implies that per-frame semantic segmentation quality is improved by effectively leveraging spatio-temporal context in training time. Furthermore, as shown in the video metric and Fig. 4, we can clearly observe that our model produce both accurate and consistent prediction compared to the baselines. Note that proposed method introduce no computational overhead in the inference time.

Ablation Study on VAT

We show the contribution of proposed component to VAT performance in Table. 3.

Method	Dice		Adv.		Metric	
	Single	Tube	Img.	Vid.	mIoU	VPQ^s
(1)					34.02	21.17
(2)			✓		43.95	29.78
(3)	✓			✓	44.03	29.51
(4)		✓	✓		44.75	30.27
Ours		✓		✓	45.53	30.81

Table 3: **Ablation study on video adversarial training.** We empirically verify the effectiveness of proposed tube matching loss and sequence discriminator.

Method	ST	Agg.	Reg.	Ref.	mIoU	VPQ^s
Video Adversarial Training					45.53	30.81
Class Balanced (Zou et al. 2018)	✓				47.63	32.26
Instance Adaptive (Mei et al. 2020)	✓				47.98	32.31
Clip Adaptive	✓				49.18	33.48
+Aggregated prediction	✓	✓			49.52	34.02
+Regularization	✓	✓	✓		51.52	35.78
+Temporal Refinement	✓	✓	✓	✓	51.90	36.43

Table 4: **Ablation study on video self-training.** “Agg.,” “Reg.” and “Ref.” denote temporally aggregated prediction, regularization and online pseudo label refinement, respectively.

Effectiveness of Tube Matching Loss. We first investigate the impact of the tube matching loss. In model-(4), We add tube matching loss on top of the image-level adaptation model(model-(2)). As improved image and video metrics indicate, we confirm that tube-matching loss helps to learn spatio-temporal knowledge in source domain, which results in powerful video domain knowledge transfer to target domain. For more comprehensive insight, we further report the result of model-(3) that involve image-level degradation of tube matching loss (e.g. $L_{tube}(P_{S,i}, y_{S,i})$). In terms of VPQ^s , model-(3) presents even worse performance than the simple image-level adaptation model. It implies that the improvements are truly based on the tube-level design of loss, not just from using the image-level dice coefficient.

Effectiveness of Sequence Discriminator. We also explore the efficacy of the sequence discriminator. Our final VAT model in Table. 3, further adopts sequence discriminator instead of image discriminator. We empirically confirm that the sequence discriminator allows better adaptation by

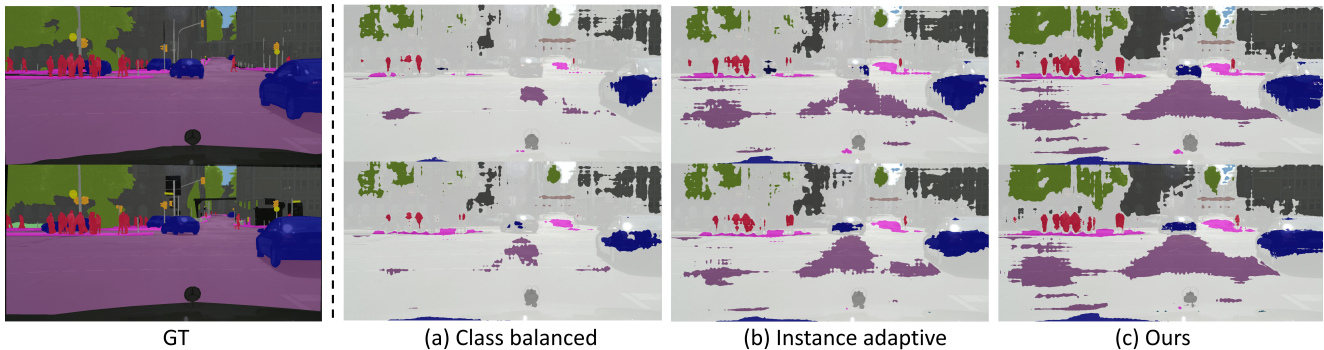


Figure 5: **Visual comparisons on pseudo labels.** We can clearly observe that proposed method generate more accurate and consistent pseudo labels over the baselines.

additionally leveraging temporal information. As a result, our VAT model achieves 1.5 mIoU and 1.0 VPQ^s over the prior adversarial method, which provides better pseudo labels to the self-training phase.

Ablation Study on VST

Effectiveness of Proposed Pseudo Label Generation Strategy. Here, we study the efficacy of clip adaptive pseudo label generation. We compare it with the previous state-of-the-art image-based pseudo label generation approaches: class-balanced (Zou et al. 2018), instance adaptive (Mei et al. 2020). As shown in the Table. 4, the model trained with the proposed clip adaptive pseudo labels shows the best performance. Plus, adopting the presented ‘temporally aggregated prediction’ further improves the performance. Finally, we also provide qualitative results in the Fig. 5. For example, both ‘‘people’’ and ‘‘car’’ classes are overlooked in previous approaches but densified with our method. Quantitatively and qualitatively, we clear see that our clip adaptive pseudo label generation generates more accurate and temporally consistent labels, which ultimately increase the performance of self training.

Importance of video adversarial training. Here we study how different first-phase adversarial methods affect the final performance. We compared them using the same video self-training in the second-phase. The results are summarized in Table. 5. Without any proposals in VAT, the final performance drop by a significant margin, showing the efficacy of our proposals. The best performance is achieved when all the proposals (i.e., tube matching and video discriminator) are used together. This again shows the importance of exploring the video context in designing the adaptation technique. We also provide qualitative pseudo labels when using IAT and VAT in Fig. 6. We obtain much dense and accurate pseudo labels with the video-level adversarial pre-training.

Visual analysis of online pseudo label refinement. We illustrate the role of online pseudo label refinement in the Fig. 3. It removes noisy pseudo labels by checking temporal consensus. For example, original pseudo labels mislabel bicycle regions as a person, while the refinement process successfully eliminates such parts. As a result, this process pre-

Adversarial Training	Self-Training	mIoU	VPQ^s
(2)	Ours	48.58	33.95
(3)	Ours	50.18	34.83
(4)	Ours	50.70	35.66
Ours	Ours	51.90	36.43

Table 5: **Importance of video adversarial training.** We run our full VST phase on the different adversarial models.

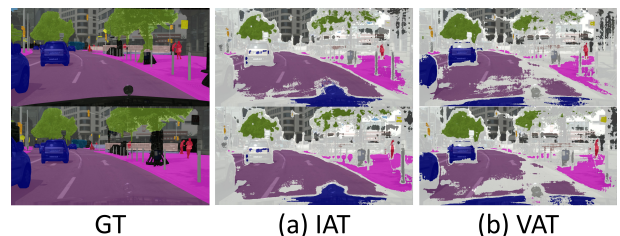


Figure 6: **Pseudo labels generated from different adversarial models.** It is obvious that the quality of generated pseudo labels depend on the pre-trained adversarial model since ours with VAT model shows better visual effect on pseudo labels than ours with IAT model.

vents the model from constantly fitting to noise, showing the better performance (Table. 4).

Conclusion

In this paper, we explore a new domain adaptation task, unsupervised domain adaptation for video semantic segmentation. We present a novel framework that consists of two video-specific domain adaptive training: VAT and VST. In the first step, we distill source knowledge using standard cross entropy loss and the newly presented tube matching loss jointly. Meanwhile, the VAT is applied for the feature alignment. In the second step, the video self-training is used for target data learning. The temporal information is leveraged to generate dense, accurate pseudo labels. We significantly outperform all the previous strong image-based UDA baselines on Viper to CityscapeVPS scenario. We hope many follow-up studies being presented in the future based on our proposals and results.

Appendices

In this supplementary section, we provide,

- A. Additional evaluations on other datasets,
- B. Comparisons with (Chen et al. 2020)
- C. Details of a new UDA framework that supports multiple popular UDA approaches in a unified platform,
- D. The impact of online pseudo label refinement,
- E. Additional analyses of the pseudo labels,
- F. Limitations and discussions of the proposals,
- G. More qualitative adaptation results on Cityscape-VPS.

A. Additional Evaluations on Other Datasets

To show that our proposal is indeed general across the datasets, we additionally evaluate our method and baselines on two more benchmarks: (a) weather adaptation: CamVid-Sunny to CamVid-Foggy and (b) synthetic-to-real: SYNTHIA-Seq to Cityscape-VPS.

For CamVid (Brostow, Fauqueur, and Cipolla 2009), it contains 5 video sequences of a total of 701 annotated frames. we use 4 sunny video as the source domain and 1 foggy video as the target domain. We compare the proposed method with the state-of-the-art baselines in the Table. 8 and Table. 9. Synthia-Seq (Ros et al. 2016) has 7 video sequences under different scenarios and traffic conditions. Among them, We only take 1928 images captured on virtual city as source domain. Experimental results are shown in the Table. 10 and Table. 11. We can see that our proposal consistently achieves the state of the art on the proposed benchmarks.

B. Comparisons with (Chen et al. 2020)

In the main paper, we claim that their framework shows inferior performance on complex video semantic segmentation. To provide experimental evidence, we conduct quantitative comparisons with (Chen et al. 2020) on CamVid-Sunny to CamVid-Foggy. For fair comparisons, we run our method in the similar setting with (Chen et al. 2020). Specifically, we adopt PSPNet (Zhao et al. 2017) as a segmentation model with ResNet-50 backbone. The results are shown in the Table. 12. The proposed method outperforms (Chen et al. 2020) with healthy margins.

C. New UDA framework

One of the paper’s main contributions is presenting a new UDA framework that supports multiple popular and contemporary UDA approaches for semantic segmentation. Specifically, our framework contains eight strong UDA baselines in a unified platform. A list is given as follows,

Adversarial-based

- AdaptSegNet (Tsai et al. 2018): adapting structured output semantic segmentation logits, proposed in 2018.
- Advent (Vu et al. 2019): adapting entropy maps, proposed in 2019.

Self-training-based

- CBST (Zou et al. 2018): class-balanced pseudo label generation, proposed in 2018.
- CRST (Zou et al. 2019): confidence regularized self-training, proposed in 2019.
- FDA (Yang and Soatto 2020): fourier domain adaptation for semantic segmentation, proposed in 2020.
- CCM (Li et al. 2020): content-consistent matching for domain adaptive semantic segmentation, proposed in 2020.

Combining above two methods

- IntraDA (Pan et al. 2020): unsupervised intra-domain adaptation for semantic segmentation through self-supervision, proposed in 2020.
- IAST (Mei et al. 2020): instance adaptive pseudo label generation, proposed in 2020.

We believe this framework is by far the first complete UDA toolbox. Upon this framework, we developed our new proposals, video adversarial training (VAT) and video self-training (VST), and enabled fair apple-to-apple comparisons. The codes and models will be released.

D. The impact of online pseudo label refinement

In the main paper, we exploit the temporal information in pseudo label generation so that the temporally inconsistent labels are *cut-out*. Another reasonable baseline is to directly borrow the reference information to *fill-in* the missing labels in current frame. In practice, we propagate the pseudo label information in the reference frame ($\hat{y}_{T,t-\tau}$) to the target frame ($\hat{y}_{T,t}$) using flow-based warping function ($W_{t-\tau \Rightarrow t}$). The overall procedure can be formulated as,

$$\begin{aligned} Prop(\hat{y}_{T,t}) &= \mathbb{R}_{T,t} * \hat{y}_{T,t} \\ &+ (1 - \mathbb{R}_{T,t}) * \mathbb{I}_{t-\tau \Rightarrow t} * W_{t-\tau \Rightarrow t}(\hat{y}_{T,t-\tau}) \end{aligned} \quad (14)$$

where $\mathbb{R}_{T,t} = \{\mathbf{1} | \hat{y}_t^{(h,w)} \neq 0\}$ is pseudo label region of current image, $\mathbb{I}_{t-\tau \Rightarrow t}$ is the non-occluded map from $x_{T,t-\tau}$ to $x_{T,t}$ and $*$ represents element-wise multiplication.

The comparison results are summarized in Table. 6. We observe that *fill-in* approach is inferior to the baseline, whereas the proposed *cut-out* algorithm shows improvement over it. We see this phenomenon comes from the in-nature noise in the pseudo label, and thus cut-out-based regularization is better than fill-in-based label accumulation. To back our claim, we also provide qualitative results in Fig. 7. We can observe the general tendency that our cut-out based label refinement less accumulates erroneous labels than the fill-in based approach.

E. Additional analysis of Pseudo Labels

In the main paper, we already highlight the effectiveness of the proposed pseudo label generation strategy by showing quantitative and qualitative comparisons in Table 4 and Figure 5. Besides, we measure mIoU of different pseudo labels and name it as P-mIoU. For fair comparisons, We tune

Method	mIoU	VPQ^s
Base	51.52	35.78
Base+fill-in	50.0	34.78
Base+cut-out (ours)	51.91	36.43

Table 6: **Comparative performance on online refinement.** We experiment different online refinement methods on top of proposed VAT and VST.

	Proportion	Methods		
		CB	IA	Ours
P-mIoU	0.3	67.8	67.9	68.8
	0.4	64.8	66.4	67.1

Table 7: **P-mIoU of different pseudo labels.** CB and IA denote class balanced (Zou et al. 2018) and instance adaptive (Mei et al. 2020) pseudo label generation methods, respectively.

the hyperparameter α (see Preliminary in the main paper) of each method to have the same proportion of pseudo labels. The results are in the Table. 7. We again observe that our proposal generates the most accurate pseudo labels regardless of the proportion. It implies that leveraging the additional temporal information is essential.

F. Qualitative results with Video Demo

We release video results ² on test sets of cityscapes dataset (Cordts et al. 2016). Our method shows much clear and consistent prediction compared to state-of-the-art image UDA method, confirming its robustness and effectiveness.

G. Limitations and Discussions

In order to make the proposed video UDA framework more competitive and facilitate the future research, we point out a few specific items that call for continuing efforts:

- **FlowNet dependency.** Currently, the overall pseudo label generation in our framework highly relies on the FlowNet (Ilg et al. 2016), which is trained on the external simulated data. This inevitably brings inferior adaptation results on certain classes that the FlowNet cannot capture well. For example, in Fig. 8, we see that the adaptation results of “Sidewalk” class is inferior to IAST framework (Mei et al. 2020) (see Fig. 8 (d)-(f)), which originates from the imperfect pseudo labels (see Fig. 8 (a)-(c)). One possible strategy might be learn to adapt without the FlowNet. We expect deeper explorations in this directions in the future.
- **How to select the initial model for VST.** As pointed out in Figure 6 of the main paper, the quality of the pseudo labels largely depends on the initial model. Even with the same adversarial methods, it is hard to select the best iteration without target domain labels due to the unstable training of adversarial methods. Thus, for the better final performance, it is unclear that what criteria to choose the model by. While this issue is an inherent limitation

of “Adversarial-then-Self training” framework itself, it is also important for better video DA methods.

References

- Brostow, G. J.; Fauqueur, J.; and Cipolla, R. 2009. Semantic object classes in video: A high-definition ground truth database. *Pattern Recognition Letters*, 30(2): 88–97.
- Chen, J.; Li, Y.; Ma, K.; and Zheng, Y. 2020. Generative adversarial networks for video-to-video domain adaptation. In *Proceedings of the AAAI Conference on Artificial Intelligence*, volume 34, 3462–3469.
- Chen, L.-C.; Papandreou, G.; Kokkinos, I.; Murphy, K.; and Yuille, A. L. 2017. DeepLab: Semantic Image Segmentation with Deep Convolutional Nets, Atrous Convolution, and Fully Connected CRFs. arXiv:1606.00915.
- Cordts, M.; Omran, M.; Ramos, S.; Rehfeld, T.; Enzweiler, M.; Benenson, R.; Franke, U.; Roth, S.; and Schiele, B. 2016. The Cityscapes Dataset for Semantic Urban Scene Understanding. In *Proc. of the IEEE Conference on Computer Vision and Pattern Recognition (CVPR)*.
- He, K.; Zhang, X.; Ren, S.; and Sun, J. 2015. Deep Residual Learning for Image Recognition. arXiv:1512.03385.
- Ilg, E.; Mayer, N.; Saikia, T.; Keuper, M.; Dosovitskiy, A.; and Brox, T. 2016. FlowNet 2.0: Evolution of Optical Flow Estimation with Deep Networks. arXiv:1612.01925.
- Kim, D.; Woo, S.; Lee, J.-Y.; and Kweon, I. S. 2020. Video Panoptic Segmentation. In *Proceedings of the IEEE Conference on Computer Vision and Pattern Recognition*.
- Li, G.; Kang, G.; Liu, W.; Wei, Y.; and Yang, Y. 2020. Content-consistent matching for domain adaptive semantic segmentation. In *Proc. of European Conf. on Computer Vision (ECCV)*, 440–456. Springer.
- Li, Y.; Shi, J.; and Lin, D. 2018. Low-latency video semantic segmentation. In *Proc. of Computer Vision and Pattern Recognition (CVPR)*, 5997–6005.
- Li, Y.; Yuan, L.; and Vasconcelos, N. 2019. Bidirectional learning for domain adaptation of semantic segmentation. In *Proceedings of the IEEE/CVF Conference on Computer Vision and Pattern Recognition*, 6936–6945.
- Liu, Y.; Shen, C.; Yu, C.; and Wang, J. 2020. Efficient Semantic Video Segmentation with Per-frame Inference. arXiv:2002.11433.
- Mei, K.; Zhu, C.; Zou, J.; and Zhang, S. 2020. Instance adaptive self-training for unsupervised domain adaptation. *arXiv preprint arXiv:2008.12197*.
- Milletari, F.; Navab, N.; and Ahmadi, S.-A. 2016. V-Net: Fully Convolutional Neural Networks for Volumetric Medical Image Segmentation. arXiv:1606.04797.
- Nilsson, D.; and Sminchisescu, C. 2017. Semantic Video Segmentation by Gated Recurrent Flow Propagation. arXiv:1612.08871.
- Pan, F.; Shin, I.; Rameau, F.; Lee, S.; and Kweon, I. S. 2020. Unsupervised intra-domain adaptation for semantic segmentation through self-supervision. In *Proceedings of the IEEE/CVF Conference on Computer Vision and Pattern Recognition*, 3764–3773.

²<https://youtu.be/z-rBcY87XCw>

Richter, S. R.; Hayder, Z.; and Koltun, V. 2017. Playing for benchmarks. In *Proceedings of the IEEE International Conference on Computer Vision*, 2213–2222.

Ros, G.; Sellart, L.; Materzynska, J.; Vazquez, D.; and Lopez, A. M. 2016. The synthia dataset: A large collection of synthetic images for semantic segmentation of urban scenes. In *Proceedings of the IEEE conference on computer vision and pattern recognition*, 3234–3243.

Sankaranarayanan, S.; Balaji, Y.; Jain, A.; Lim, S. N.; and Chellappa, R. 2018. Learning from Synthetic Data: Addressing Domain Shift for Semantic Segmentation. arXiv:1711.06969.

Shelhamer, E.; Rakelly, K.; Hoffman, J.; and Darrell, T. 2016. Clockwork Convnets for Video Semantic Segmentation. arXiv:1608.03609.

Shin, I.; Woo, S.; Pan, F.; and Kweon, I. S. 2020. Two-phase Pseudo Label Densification for Self-training based Domain Adaptation. In *European Conference on Computer Vision*, 532–548. Springer.

Tsai, Y.-H.; Hung, W.-C.; Schuster, S.; Sohn, K.; Yang, M.-H.; and Chandraker, M. 2018. Learning to adapt structured output space for semantic segmentation. In *Proc. of Computer Vision and Pattern Recognition (CVPR)*, 7472–7481.

Vu, T.-H.; Jain, H.; Bucher, M.; Cord, M.; and Pérez, P. 2019. Advent: Adversarial entropy minimization for domain adaptation in semantic segmentation. In *Proceedings of the IEEE/CVF Conference on Computer Vision and Pattern Recognition*, 2517–2526.

Wang, Z.; Yu, M.; Wei, Y.; Feris, R.; Xiong, J.; mei Hwu, W.; Huang, T. S.; and Shi, H. 2020. Differential Treatment for Stuff and Things: A Simple Unsupervised Domain Adaptation Method for Semantic Segmentation. arXiv:2003.08040.

Yang, Y.; and Soatto, S. 2020. Fda: Fourier domain adaptation for semantic segmentation. In *Proc. of Computer Vision and Pattern Recognition (CVPR)*, 4085–4095.

Yu, F.; Chen, H.; Wang, X.; Xian, W.; Chen, Y.; Liu, F.; Madhavan, V.; and Darrell, T. 2020. Bdd100k: A diverse driving dataset for heterogeneous multitask learning. In *Proc. of Computer Vision and Pattern Recognition (CVPR)*, 2636–2645.

Zhao, H.; Shi, J.; Qi, X.; Wang, X.; and Jia, J. 2017. Pyramid scene parsing network. In *Proceedings of the IEEE conference on computer vision and pattern recognition*, 2881–2890.

Zhu, X.; Xiong, Y.; Dai, J.; Yuan, L.; and Wei, Y. 2017. Deep Feature Flow for Video Recognition. arXiv:1611.07715.

Zou, Y.; Yu, Z.; Kumar, B.; and Wang, J. 2018. Domain adaptation for semantic segmentation via class-balanced self-training. arXiv preprint arXiv:1810.07911.

Zou, Y.; Yu, Z.; Liu, X.; Kumar, B.; and Wang, J. 2019. Confidence regularized self-training. In *Proceedings of the IEEE/CVF International Conference on Computer Vision*, 5982–5991.

CamVid-Sunny → CamVid-Foggy [mIoU]													
Method	Arch.	Bicyclist	Building	Car	Pole	Fence	Pedestrian	Road	Sidewalk	Sign	Sky	Tree	mIOU(%)
Source-only	-	56.08	64.80	82.97	18.56	23.87	53.05	87.93	63.08	8.45	50.16	68.92	52.54
AdaptSegNet (Tsai et al. 2018)	AT	47.44	78.98	74.48	12.30	26.25	43.52	82.02	54.73	4.66	86.84	77.73	53.54
Advent (Vu et al. 2019)	AT	46.62	79.32	74.70	11.94	25.16	43.30	81.83	54.82	4.40	87.30	77.79	53.38
CBST* (Zou et al. 2018)	A+S	65.40	84.61	85.50	24.59	40.13	61.34	89.73	74.41	5.42	91.27	80.33	63.88
CRST* (Zou et al. 2019)	A+S	65.93	84.48	85.64	24.84	39.90	61.72	89.66	74.26	5.33	91.22	80.50	63.95
IAST (Mei et al. 2020)	A+S	65.35	85.00	86.60	21.65	39.87	60.88	90.34	72.21	7.10	91.36	80.89	63.75
Ours	A+S	69.78	85.19	86.48	24.35	40.21	61.72	91.36	76.64	10.75	91.54	81.79	65.44

Table 8: Image semantic segmentation results(mIoU) on CamVid-Sunny → CamVid-Foggy.

CamVid-Sunny → CamVid-Foggy [VPQ ^s]													
Method	Arch.	Bicyclist	Building	Car	Pole	Fence	Pedestrian	Road	Sidewalk	Sign	Sky	Tree	VPQ ^s (%)
Source-only	-	28.36	48.31	79.93	0.71	3.20	26.10	87.15	51.57	3.16	32.26	50.10	37.35
AdaptSegNet (Tsai et al. 2018)	AT	13.62	66.26	68.68	0.0	7.92	19.55	80.53	34.95	0.0	86.74	60.67	39.90
Advent (Vu et al. 2019)	AT	12.82	66.60	68.71	0.0	7.59	19.33	80.33	34.93	0.0	87.23	60.73	39.84
CBST* (Zou et al. 2018)	A+S	38.05	74.75	83.02	2.01	23.85	37.11	88.97	71.22	1.81	91.26	70.32	52.94
CRST* (Zou et al. 2019)	A+S	38.00	74.93	83.17	2.01	23.25	37.98	88.85	71.17	1.81	91.20	70.87	53.02
IAST (Mei et al. 2020)	A+S	38.55	76.44	83.82	1.66	22.48	38.16	89.69	68.57	3.72	91.41	71.32	53.26
Ours	A+S	46.93	76.86	83.47	2.07	23.79	39.40	90.72	73.29	5.20	91.63	72.75	55.10

Table 9: Video semantic segmentation results(VPQ^s) on CamVid-Sunny → CamVid-Foggy.

SYNTHIA-Seq → Cityscapes-VPS [mIoU]													
Method	Arch.	road	sidewalk	building	pole	light	sign	vegetation	sky	person	rider	car	mIOU(%)
Source-only	-	79.00	34.31	72.30	23.51	11.36	28.13	72.08	72.75	57.82	10.46	64.24	47.81
AdaptSegNet (Tsai et al. 2018)	AT	85.29	40.14	77.26	22.08	9.03	27.96	72.12	68.06	58.93	0.0	75.49	48.76
Advent (Vu et al. 2019)	AT	84.02	37.50	76.54	21.52	8.22	27.56	71.76	68.17	57.40	0.0	75.24	47.99
CBST* (Zou et al. 2018)	A+S	87.61	43.96	77.81	32.46	23.43	35.59	75.34	79.68	56.03	10.03	81.44	54.85
CRST* (Zou et al. 2019)	A+S	86.07	43.77	79.12	31.17	27.47	38.94	77.11	80.47	59.48	12.47	82.43	56.23
IAST (Mei et al. 2020)	A+S	88.34	48.68	80.42	34.19	28.88	39.51	79.74	77.27	59.30	9.36	83.05	57.16
Ours	A+S	89.84	50.51	81.46	32.98	30.27	40.39	80.91	81.13	59.87	8.79	84.40	58.23

Table 10: Image semantic segmentation results(mIoU) on SYNTHIA-Seq → Cityscapes-VPS benchmark.

SYNTHIA-Seq → Cityscapes-VPS [VPQ ^s]													
Method	Arch.	road	sidewalk	building	pole	light	sign	vegetation	sky	person	rider	car	VPQ ^s (%)
Source-only	-	76.02	16.89	62.67	0.64	1.49	6.40	59.59	61.39	17.10	0.0	50.62	32.07
AdaptSegNet (Tsai et al. 2018)	AT	84.59	19.15	66.34	0.10	0.25	6.14	57.95	59.21	17.95	0.0	62.90	34.05
Advent (Vu et al. 2019)	AT	83.23	15.89	65.44	0.04	0.17	5.68	56.80	59.43	17.14	0.0	62.40	33.29
CBST* (Zou et al. 2018)	A+S	84.98	28.85	70.48	2.29	1.79	9.78	64.58	67.74	24.17	0.0	69.47	38.56
CRST* (Zou et al. 2019)	A+S	83.49	33.70	71.79	1.01	2.11	13.56	69.23	69.08	23.33	0.0	73.11	40.04
IAST (Mei et al. 2020)	A+S	85.74	37.25	73.36	4.42	3.07	13.89	73.08	70.12	26.79	0.0	73.34	41.92
Ours	A+S	88.15	39.20	75.04	4.17	4.36	14.89	74.93	73.10	28.75	0.0	73.70	43.30

Table 11: Video semantic segmentation results(VPQ^s) on SYNTHIA-Seq → Cityscapes-VPS benchmark.

CamVid-Sunny → CamVid-Foggy [mIoU]													
Method	Arch.	Bicyclist	Building	Car	Pole	Fence	Pedestrian	Road	Sidewalk	Sign	Sky	Tree	mIOU(%)
Source-only	-	4.19	35.34	35.55	8.31	2.14	22.63	54.07	45.70	9.63	5.17	37.61	23.49
VideoGAN (Chen et al. 2020)	-	8.98	50.44	37.24	15.27	2.84	31.62	58.33	62.63	3.45	49.68	62.77	34.18
Source-only†	-	5.91	50.37	33.42	0.03	0.0	0.1	44.86	22.48	0.02	47.15	37.90	22.02
Ours	A+S	16.76	70.81	44.94	0.49	19.5	17.22	41.23	41.07	0.0	86.31	69.01	43.82

Table 12: Quantitative comparisons of ours with (Chen et al. 2020) on CamVid-Sunny → CamVid-Foggy. † denotes the source only model reproduced in this paper.

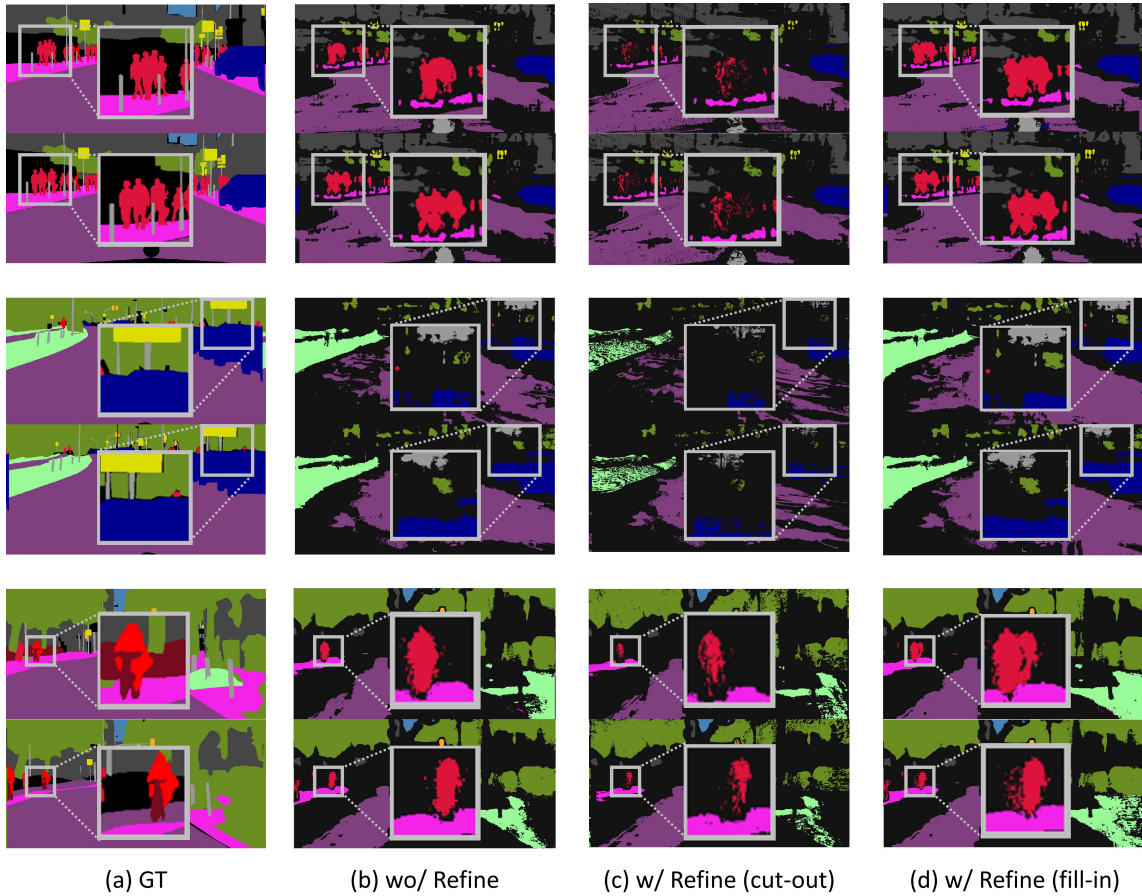


Figure 7: **Visualization of pseudo-labels w/o and w/ the online refinements.** The proposed *cut-out* refinement successfully eliminate noise on the pseudo labels by checking temporal consensus. However, *fill-in* based method makes additional noise on pseudo labels.

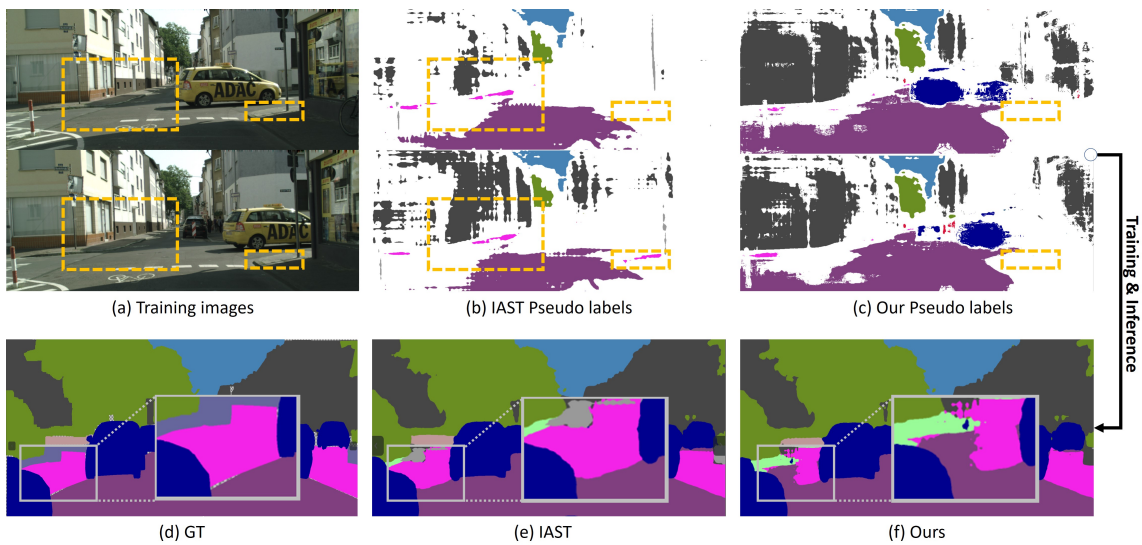


Figure 8: **Visualization of cause and effect in our failure case.** Our model is comparably weak to certain class, which could be originated from pseudo label generation process. Detail analysis is on Sec.F